Supporting Information

Zeharia et al. 10.1073/pnas.1119125109

SI Text

Periodic Experiments. ***Start Toes experiment.*** Subjects moved 20 body parts consecutively while lying with their eyes closed and blindfolded inside the functional MRI scanner. The movement sequence followed the spatial order from toes to tongue found by Penfield in the primary motor cortex homunculus. It included bilateral/axial movements of the following body parts: toes (flexion/extension), feet (flexion/extension), thighs (contraction), buttocks (contraction), stomach (contraction), upper arm (contraction), elbow (flexion/extension), wrist (flexion/extension), fist (contraction), little finger (flexion/extension), ring finger (flexion/extension), middle finger (flexion/extension), index finger (flexion/extension), thumb (flexion/extension), forehead (contraction), nose (contraction), eyelids (contraction), lips (contraction), jaw (flexion/extension), and tongue (a side to side movement with closed mouth). The subjects were instructed to execute the movements on hearing an auditory cue, which was the spoken name of the body part followed by three metronome beeps at 1-s intervals, during which time the subject moved. Overall, each body part was moved three times within a period of 3 s; the next body part was announced during the last 1 s. The whole movement cycle lasted 60 s and was followed by a rest period of 12 s. Eight cycles of movement and rest were performed, resulting in a stimulus frequency of 0.0138 Hz. The subjects were trained for approximately 1 h before entering the scanner. During training, their movements were recorded by the Polhemus LIBERTY 240/16 tracking device to ensure that they were able to perform the movements perfectly and that the only body parts moved were as per instructions. In two subjects, electromyographs (EMGs) were recorded during the scan.

Start Tongue experiment. Eight of eleven subjects who participated in the Start Toes experiment also participated in this experiment. This experiment was identical to the Start Toes experiment, but the movements were performed in the reverse order from tongue to toes.

Data were analyzed separately for each direction in the periodic experiment and gave very similar results. To minimize order effects, we pooled data from the two directions (Start Toes and Start Tongue).

Slow Event-Related Experiment. Seven subjects participated in a slow event-related paradigm experiment (two of the subjects also participated in the periodic experiments). A 4.5-s block of movement was followed by a 12-s rest. At the beginning of each movement period, subjects heard the name of the body part to be moved. Movement was paced with a metronome, which continued beating during the rest period. All 20 body parts moved in the periodic experiments were moved 20 times in a pseudorandomized order balanced for history. The 400 movement–rest periods were divided into 10 sessions. After five sessions, subjects left the scanner for 20 min and then returned for the remaining five sessions. In five subjects, EMGs were recorded.

Block Design. The seven subjects who participated in the slow event-related experiment also participated in the block design experiment. In each block, the subjects were instructed to perform a bilateral or centralized movement of one of three body parts: feet (flexion/extension), hands (flexion/extension of the wrist), and tongue (side to side movement with mouth closed). Each condition appeared eight times in a pseudorandomized order. As in the previous experiments, subjects were blindfolded, and the movements were guided by an auditory cue. At the beginning of each movement block, subjects heard the name of the body part. Each block lasted 9 s, and during the block, the movements were paced at 1 Hz by a metronome. Each movement block was followed by 9-s rest in which subjects heard the metronome but were instructed not to move.

Contribution of the Different Designs. The results of both the positive and negative blood oxygenation level-dependent (BOLD) patterns were highly consistent across the different designs. However, each of these designs has advantages and disadvantages, and associating the three results enables a comprehensive picture of positive and negative BOLD in the primary motor cortex (M1) and supplementary motor area (SMA).

The block design and the event-related experiments allowed a clean analysis of the negative BOLD (Figs. 2–4), which is defined as a reduction in the BOLD signal relative to the rest baseline.

In these designs (in contrast to the periodic design), the movement of each body part was followed by a relatively long rest period in which no movement was executed, making it possible to contrast movement vs. rest. This design also allowed for a clear presentation of the positive and negative time courses during movement.

In addition, unlike the periodic designs, the order of movements in these two experiments was randomized, and therefore, any concerns regarding an interaction between neuronal activity during movement of different body parts was addressed. This is especially important in the case of multivoxel pattern analysis (MVPA).

The following reasons are the reasons why we chose to use these two designs and not just one of them.

A block design usually affords a better signal-to-noise ratio than an event-related design, and it is also the most frequently used and verified experimental design in the literature.

The block design experiment also enabled us to perform regions of interest (ROIs) analysis of the general linear model (GLM) parameter estimators and the time courses without voxel hunting by using the block design as an external localizer (Fig. 2*C*).

The use of an event-related design containing movements of 20 body parts allowed for a full and detailed depiction of the positive and negative BOLD along M1 for all these body parts, which was seen in the ROI analysis (Fig. 2*C*). This design allowed us to confirm that significant information (either a significant reduction or a significant increase in the BOLD signal) could be found across M1 during the movement of a single body part and that this phenomenon was not restricted to a limited number of body parts.

In addition, the use of a random event-related design with 20 body parts allowed us to carry out an MVPA. MVPA was used to predict which body part was being moved based on the BOLD signal in M1 and the SMA. This prediction cannot be done using an ordered periodic design; thus, we had to use a randomized design. Furthermore, in this analysis, we predicted the identity of the moving body part from among a group of nearby body parts. Therefore, the use of a limited number of body parts as in the block design experiment was not possible, and instead, we used a design with a large number of body parts that was divided into face, hand, and leg and trunk body parts. This design enabled us to deduce that somatotopic information exists in the positive BOLD in M1 and the SMA as well as in the negative BOLD in M1 (Fig. 4).

The periodic design enabled us to use phase-locked analysis approaches (spectral analysis and cross-correlation analysis, which are presented in Fig. 1 *B*, *C*, and *F*). A similar periodic design and phase-locked analysis have been used for retinotopic, somatosensory and auditory mapping.

These phase-locked analysis methods are optimal for topographical mapping, and we, therefore, found them particularly well-suited for detailed, whole-body mapping of the motor somatototopy in M1 and the SMA. However, these methods require the body parts to be organized in a highly ordered fashion. To partly overcome this problem, we used both directions—Start Toes and Start Tongue—but to fully control for the order effect, we used randomized designs as stated above.

The periodic experiments were not used to define negative and positive BOLD because of the lack of rest period between movements of adjacent body parts in this design.

EMG Measurements and Analysis. EMG measurements were recorded from two subjects in the periodic experiments and five other subjects in the slow event-related experiment. MRI-compatible surface EMG electrodes (MP150 data acquisition system; BIOPAC Systems, Inc.) were used to record muscle activity during the functional MRI scan from one of the following four muscles: the right or left biceps brachii muscle or the right or left quadriceps muscle. In the slow event-related experiment, the EMG signal was recorded from different muscles in different sessions for each subject. The temporal resolution was 400 Hz. The signal was filtered using Acknowledge software (version 4.1.1) in the frequencies of the TR (0.666 Hz) and the interslice time (17.54 Hz) to reduce scan-related noise. EMG recordings at the movement time of each of the 20 body parts were averaged across its repetitions and represented as separate graphs (Figs. S1 and S2).

Functional MRI Acquisition. The BOLD functional MRI measurements were obtained in a whole-body 3T Magnetom Trio scanner (Siemens). The functional MRI protocols were based on multislice gradient echoplanar imaging and a standard head coil. The functional data were collected under the following timing parameters: TR = 1.5 s, Echo Time (TE) = 30 ms, Flip Angle (FA) = 70°, imaging matrix = 80 × 80, field of view = 24 × 24 cm (i.e., in-plane resolution of 3 mm). We used a relatively short TR value to later superimpose the phase-locking spectral analysis approach; 26 slices with slice thickness of 4.5 mm and no gap were oriented in the axial position for complete coverage of the cortex.

3D Recording and Cortex Reconstruction. Separate 3D recordings were used for coregistration. High-resolution 3D anatomical volumes were collected using T1-weighted images with a 3D turbo field echo T1-weighted sequence [equivalent to magnetization-prepared rapid acquisition with gradient echo (MP-RAGE)]. Typical parameters were field of view: 23 right–left (RL) × 23 ventral–dorsal (VD) × 17 anterior–posterior (AP) cm; foldover axis: RL; data matrix: 160 × 160 × 144 zero-filled to 256 in all directions (approximately 1 mm isovoxel native data); TR/TE = 9/6 ms; and flip angle = 8°. Group results were superimposed on a 3D cortical reconstruction of a Talairach normalized brain. Cortical reconstruction included the segmentation of the white matter using a grow region function embedded in the Brain Voyager QX 2.1.2 software package. The cortical surface was then inflated.

Preprocessing. The first 10 images (during the first baseline rest condition) were excluded from the analysis in all experiments because of nonsteady state magnetization. Data were mainly preprocessed using the Brain Voyager QX software package (Brain Innovation). Functional MRI data preprocessing included head motion correction (exclusion criterion was head movements of more than 1 voxel). Slice scan time correction and high-pass filtering using temporal smoothing in the frequency domain removed drifts and improved the signal-to-noise ratio. Functional and anatomical datasets for each subject were aligned and fitted to standardized Talairach space.

GLM Analysis. This analysis assessed somatotopy and positive and negative BOLD. The predictors were defined as a canonical hemodynamic response function convolved with a square-wave function representing the movement time, whereas the rest period was modeled implicitly. For group analysis, we used a Gaussian 8-mm filter for spatial smoothing. Cross-subject statistical parametric maps were calculated using a hierarchical random effects model analysis.

Spectral Analyses. Spectral analyses were conducted with an in-house program using MATLAB (MathWorks). Using standard retinotopy procedures, we applied Fourier analysis to retrieve responses that were locked to the movement repetition frequency.

Before the Fourier analysis, time courses were detrended to remove mean value and linear drifts. The complex Fourier coefficient at the repetition frequency f_{rep} of interest is denoted by (Eq. **S1**)

$$F(f_{rep}) \equiv a(f_{rep}) \cdot e^{i \cdot \varphi(f_{rep})}, \qquad \textbf{[S1]}$$

where $a(f_{rep})$ represents the amplitude and $\varphi(f_{rep})$ represents the phase. It is calculated by (Eq. **S2**)

$$F(f_{rep}) = \sum_{k=1}^{N} TC_k \cdot e^{-2\pi i (k \cdot f_{rep})}, \qquad \textbf{[S2]}$$

where *TC* represents the sample time course with mean value removed and *N* is the number of sampled time points.

Both the amplitude and phase parameters were used to construct a pure cosine, which served as a model of the activation (Eq. **S3**). A Pearson correlation coefficient was then calculated between the model and the original time course. This procedure resulted in a correlation coefficient for each voxel. This correlation coefficient can also be written as a normalized Fourier coefficient (Eq. **S3**):

$$Model_{f_{rep}} \equiv a(f_{rep}) \cdot \cos(2\pi f_{rep} \cdot t + \varphi(f_{rep})) \qquad \textbf{[S3]}$$

and (Eq. **S4**)

$$R(f_{rep}) \equiv \sqrt{\frac{TC \cdot Model_{f_{rep}}}{\|TC\| \cdot \left\|Model_{f_{rep}}\right\|}} = \frac{a(f_{rep})}{\sqrt{\sum_{k=1}^{N} a(f_k)^2}}. \qquad \textbf{[S4]}$$

On the single-subject level, the correlation coefficient was used as a direct measure of the voxel's response to the movement of interest. In regions showing a high correlation to the movement repetition frequency, the phase value was inspected. Phase values were distributed between $-\pi$ and π, and they were linearly transformed to represent the time points in each movement cycle.

The results from single subjects were analyzed in both spatially smoothed [(Gaussian kernel of 4 mm full width at half maximum (FWHM), which were used later for group analysis] and unsmoothed data (Figs. S5 and S6) to ensure that the somatotopic gradient was not the result of spatial smoothing of the signal.

On the group level, to run the random effect analysis, we used GLM parameter estimators derived from a complementary analysis as follows. First, a GLM analysis was carried out at the single-subject level using the pure cosine model described above as a predictor. The pure cosine model predictor is positively biased, because it is derived from the Fourier analysis (as described above). To account for this bias, we applied the same approach to

20 other nonstimulus-related frequencies for each subject. The average GLM parameter estimator value from these analyses was used as the bias estimator and subtracted from the GLM parameter estimator values from individuals in the stimulus representation frequency. The resulted GLM parameter estimator values were then used in a second-level analysis for the group random effect. Finally, the random effect results were corrected for multiple comparisons using the Monte Carlo method (1,000 iterations, $\alpha < 0.05$) with a priori threshold of $P < 0.05$.

The phase maps of the individual subjects were averaged using a circular average method to create a mean phase map. These phase values were distributed between $-\pi$ and π, and they were linearly transformed to represent the time points in each movement cycle. Because of the time delay of the hemodynamic response, the phase code does not temporally overlap with the movement time. The earliest response detected in the anatomically defined primary motor cortex was assumed to correspond to toe movement (in the Start Toes experiment) or tongue movement (in the Start Tongue experiment), which was the first movement in the movement cycle. Similarly, the latest response was assumed to correspond to the last movement in the movement cycle. The hemodynamic response was assumed to be spatially uniform, thus leading us to interpret latencies between the shortest and latest responses as driven from movements of intermediate body parts. These values constructed the phase code corresponding to the specific preferred body part of each voxel. The phase maps were thresholded by both the averaged correlation coefficient map and the random effect corrected for multiple comparison map.

Map Alignment Measure. To quantify the compatibility between the spectral analysis somatotopic map and the cross-correlation map, we used an alignment index (Fig. 1). The alignment index was calculated voxelwise as (Eq. **S5**)

$$Alignment\_Index = 1 - \frac{|\Delta\phi|}{\pi}, \qquad \textbf{[S5]}$$

where $\Delta\phi$ is the difference between the phases of two voxels. This index is one when the phases are identical across the maps and zero when the phases are opposite of one another. The similarity of two maps can, therefore, be evaluated by comparing the distribution of its alignment indices with the distribution of random maps. If the maps are similar, the alignment indices will be distributed with a sharp peak to one. Random map indices are distributed with linear increase to one. The difference between these distributions was assessed statistically.

ROI Analysis. ROIs were defined at the group level from the block design experiment, which served here as an external localizer experiment. Six ROIs in every homunculus and each hemisphere were defined from the dorsal and ventral peaks of negative BOLD of legs, hands, and tongue movements vs. rest baseline.

GLM analysis was performed in each ROI, yielding the GLM parameter estimators of movements of each of the body parts vs. rest baseline in the slow event-related experiment or event-related averaging of the time course of the slow event-related experiment separately for legs, hands, and face body parts.

Multivoxel Pattern Analysis. We used a multiclass support vector machine (SVM) to classify the data of the body parts in different ROIs in M1 and the SMA (Fig. 4). The classification was carried out in ROIs that were defined functionally and constrained by the anatomical position of the central sulcus or Brodmann area 6 in the medial wall (separately for each subject) to ensure that the data used for classification were, indeed, positive or negative BOLD. The ROIs were defined as significantly activated voxels in the contrast legs, hands, or face vs. the rest baseline in the event-related experiment, which were located on the anterior bank of the central sulcus or medial Brodmann area 6, as well as deactivated voxels on the anterior bank of the central sulcus or the lateral parietal area in the default system.

In contrast to the Monte Carlo correction of the statistical parametric maps, the correction for multiple comparisons of the ROIs used for the MVPA was done on the voxel level using the FDR method with $\alpha < 0.05$. We chose this method to ensure that each voxel (feature) used for classification was, indeed, significantly positive or negative. The uncorrected values were between $P < 0.023$ and $P < 0.039$.

In the next step, we defined the data to be classified separately for each subject. We used unsmoothed data to preserve the signal's distributed spatial pattern and avoid leakage of information from the positive to negative BOLD. For each of the trials in the slow event-related experiment, we obtained a GLM parameter estimator value in each voxel. This yielded 20×20 GLM parameter estimator values for each voxel in the ROI, corresponding to the 20 body parts and 20 trials for each body part. We then divided the data into three groups of neighboring body parts: five leg and trunk-related body parts (toes, feet, thighs, buttocks, and stomach), nine hand-related body parts (arm, elbow, wrist, fist, and the five fingers), and six face-related parts (forehead, nose, eyelids, lips, jaw, and tongue). The data for each trial across the different voxels were then z-scored to avoid classification because of global elevation or reduction of the signal.

We then took one group of body parts and one ROI (e.g., hand-related body parts and hand-positive BOLD M1 ROI) and used the leave one out approach for classification. We used the training data to train a linear SVM classifier with the svmtrain command in Matlab. Because there were several body parts in each group, we used a multiclass SVM, running the classification repeatedly between the different pairs of body parts within the one body part group and then testing the performances of the classifier on the test data. The classification was considered correct only when the classifier chose the correct output in all the classification pairs. The performances of the classifier given a group of body parts in a given ROI were calculated as the mean of the percentages of successful classifications of each body part within this category. The group results were obtained by averaging the classification results of the different subjects.

Significance levels were assessed by a permutation test on each group of body parts in each ROI in each subject. In this test, we randomly permutated the labels of the different categories and then trained and tested the classifier on this incorrectly labeled data. This procedure was repeated 1,500 times, resulting in a distribution of performances of the classifier. The mean of this distribution stood for the chance levels of classification and was ~1/number of categories. For each distribution, we also calculated the 95th percentile. Only if the performance of the classifier was above this percentile was the classification considered significant.

To exclude the possibility that the classification resulted from the influence of nonneuronal factors (e.g., head movements) on the classification, we also compared the accuracy of the classification results in M1 and the SMA with the accuracy of classification using signals from the ventricles, in which the signal derives purely from nonneural factors. The classification for all ROIs and all body part groups was significantly higher than in the ventricles. Thus, the accuracy of classification found in M1 and the SMA was not caused by nonneuronal factors.

As an additional control, we examined whether negative BOLD elicited by the movements outside of the motor system also enabled accurate classification. In addition to the negative BOLD in M1, the movements also elicited negative BOLD in the default system, which is also deactivated quite nonspecifically in many

other tasks. We, therefore, performed an additional control, applying MVPA to the negative BOLD signal derived from the lateral–parietal area of the default system (e.g., classifying hand body parts using negative BOLD from the lateral–parietal area of the default system elicited by hand movements). This classification was significantly lower than the classification using negative BOLD in M1 ($P < 0.004$, $P < 0.02$, and $P < 0.03$). Classification using negative BOLD from the default system did not differ significantly from the classification using BOLD signal from the ventricles ($P < 0.46$, $P < 0.06$, and $P < 0.68$ for face, hand and leg body parts, respectively). Thus, movement-elicited negative BOLD in the default system did not contain body part-specific somatotopic information.

Contribution of the Different Analyses to Somatotopic Mapping. We used three analysis methods (GLM, cross-correlation, and spectral analysis) for somatotopic motor mapping in this study. These methods are complementary, and each method has advantages and disadvantages.

Specifically, the GLM analysis is a classical analysis method in functional MRI studies, and it has been applied previously in motor somatotopic mapping with a block design approach in M1 and the SMA. GLM makes it possible to identify the peak activations of the different body parts as well as the contrasts between different body parts (i.e., finding the areas in which the movement of one body part elicits significantly greater BOLD activation than the activation elicited by the movements of other body parts).

GLM analysis was also critical in defining the negative BOLD (which is defined as a decrease in the BOLD signal during movement relative to the rest baseline), because the baseline in this analysis implicitly contains the rest periods but not the movement periods of the experiment.

However, the GLM analysis is less optimal for mapping brain areas that continuously map a certain parameter in a topographic manner. In such areas, including in M1 and the SMA, there are usually two features that appear concurrently: a gradual progression of the neuronal representation of the parameter (in this case, the body part represented) as well as an extensive overlap in representation (in this case, an overlap in the representation of the different body parts).

These two features pose a signal-to-noise difficulty for GLM analysis. First, in this analysis, each gradual change in the represented parameter (e.g., the body) is modeled separately (e.g., in our experiment, there were 20 separate predictors in the GLM, one for each body part), which results in a large number of parameters in the model. Second, because of the overlap in representation, it is often the case that the signal of each represented feature separately (e.g., each body part) is low, and therefore, the activation of a given feature relative to the rest baseline or a contrast between the activations of different features cannot always be detected.

By contrast, periodic analyses are optimal for mapping such gradual topographic representations in the brain (8), and they have been used for the mapping of retinotopic, cochleotopic, and somatosensory maps (9–11) but not motor somatotopy. Because of the assumption that the representation is continuous and topographic (which does not exist in GLM), periodic analyses are more efficient in mapping these gradients if they exist. Even if the amplitude of the response is relatively low in a certain voxel, the methods still allow for the extraction of the represented parameter (e.g., the body part represented by a phase or lag value). Therefore, these sensitive analyses require fewer repetitions and enable much faster mapping [e.g., for somatotopic mapping of 20 body parts using the slow event-related design (and GLM analysis), the scanning time for each subject was 2 h, whereas the same mapping using the periodic experiments (and the periodic analysis techniques) only took 20 min of scanning].

These advantages are critical at the single-subject level, because the variability and lower signal to noise ratio are often even more apparent at this level. The speed of scanning can be crucial as well in the case of somatotopic/motor mapping in single subjects for medical purposes (for instance, for guidance of future deep brain stimulation).

Thus, we also used two complementary periodic analyses (cross-correlation analysis and spectral analysis), which yielded very similar results (Fig. 1*D*). However, each of these analyses has slight advantages and disadvantages (especially in relation to the assumptions concerning the shape of the hemodynamic signal), and we, therefore, chose to analyze the data with both of them.

Spectral analysis seems to be highly efficient for topographic mapping and gives robust results in a short scanning time without requiring a large number of repetitions, both at the group (Fig. 1*C*) and single-subject (Figs. S5 and S6) levels.

This robustness and efficiency are also associated with a higher signal-to-noise ratio than the GLM method in the case of topographic mapping. Specifically, motor homunculi, such as M1 and the SMA, may have overlaps in the representation of different body parts. As stated above, such an overlap may pose problems when using the GLM method. In contrast, when a continuous experimental design is used, spectral analysis is much more subtle and efficient for detecting the representation in voxels with different amounts of overlap. This efficiency is because of the fact that Fourier analysis is generally less sensitive to the exact shape of the response and more driven by the periodicity and timing of the response. The shape of the hemodynamic response in a continuous experiment may vary as a function of the degree of overlap between body part representations (the response will be wider when the overlap in representation is larger). Because spectral analysis is not confined to a specific hemodynamic response function (HRF) model or shape of response, it can identify various activation shapes, including broadly tuned voxels (which are assigned intermediate phase values that average the phase values of the different body parts represented) or highly selective voxels.

In cross-correlation analysis, similar to spectral analysis, a periodic analysis is carried out, but the HRF is still taken into account. This analysis shares the robustness and efficiency relative to GLM in mapping topographic gradients described for spectral analysis. As stated above, the two methods produce highly similar results.

However, there are several differences between these two methods. Primarily, these differences arise from the fact that spectral analysis does not take into account the HRF, whereas the cross-correlation analysis does use an HRF model of activation.

The HRF predictor is the canonical predictor for modeling the hemodynamic response in the brain, and it can simulate this response quite well. However, this predictor makes the cross-correlation analysis highly sensitive to the shape of the response and the degree of overlap in representation. Given that the HRF predictor corresponds to the movement time of a single body part, this analysis is suitable when the overlap in representation is small but less adequate when the voxel is broadly tuned to movements of various body parts. This finding is also emphasized by the fact that this analysis, in contrast to the GLM and spectral analysis, is a winner takes all analysis—only one lag value corresponding to only one body part is chosen. This result may allow a clear estimation of the represented body part in each voxel but as stated above, is less optimal in cases of some overlap in the representation.

Evaluation of the Gradual Shift in Representation Using Different Analysis Methods. To evaluate the gradual shift in representation using GLM, spectral, and cross-correlation analyses, we sampled 22 consecutive regions of interest along M1 in the right and left hemispheres. We then extracted the measure of somatotopy in each of these ROIs using each of the three analysis

techniques. In the cross-correlation analysis, the measure of somatotopy is the lag value, and in the spectral analysis, this measure is the phase value. In the GLM analysis, because the analysis produces GLM parameter estimators (β-values) and *t* values vs. the rest (which are the β-values in relation to the noise) for each of the 20 body parts, we chose the body part with the highest *t* value as the measure of somatotopy (1). We then normalized these measures of somatotopy between zero and one (Fig. S4).

The graphs in Fig. S4 illustrate the fact that somatotopy using the GLM method tends to progress along the homunculus in a more jumpy or stepwise manner than the other two analyses. We quantified this difference using two measures.

As the first measure, we used the normalized sum of the second derivative of each graph separately. For the purpose of this analysis, which quantifies the degree of smoothness of the progression of somatotopy along M1, we omitted the zero values from the first derivative (which represent ROIs along M1 in which the somatotopy measure did not change) and then calculated the second derivative. The sum of the absolute value of the second derivative was normalized by the number of ROIs that was not omitted. The lower that this measure becomes, the greater the smoothness of the somatotopy. The results in the left hemisphere were 0.09 for cross-correlation analysis, 0.11 for spectral analysis, and 0.31 for GLM analysis. The results in the right hemisphere were 0.08 for cross-correlation analysis, 0.1 for spectral analysis, and 0.18 for GLM analysis. Therefore, cross-correlation and spectral analysis produce a smoother gradual shift in the somatotopic representation according to this measure.

As the second measure, we calculated the linear fit for each of the graphs separately and then calculated the residuals between this linear fit and the graph. The variance of the absolute value of these residuals served here as a measure of the smoothness of representation: as this variance gets smaller, the smoothness of somatotopy increases. The results in the left hemisphere were 0.0047 for cross-correlation analysis, 0.0045 for spectral analysis, and 0.014 for GLM analysis. The results in the right hemisphere were 0.0036 for cross-correlation analysis, 0.0025 for spectral analysis, and 0.0038 for GLM analysis. Therefore, this measure also suggests that the results of GLM analysis were generally less smooth than the results of the other two analyses, but this difference was more pronounced in the left hemisphere.

1. Meier JD, Aflalo TN, Kastner S, Graziano MSA (2008) Complex organization of human primary motor cortex: A high-resolution fMRI study. *J Neurophysiol* 100:1800–1812.

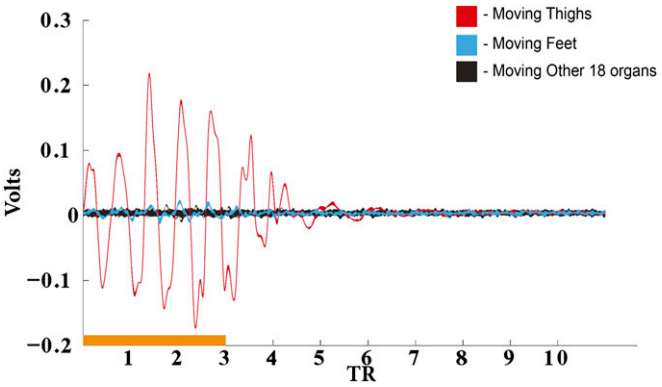

Fig. S1. EMG measurements from the quadriceps muscle of one subject when moving each of the 20 body parts in the slow event-related experiment. Orange, the duration of instructed movement.

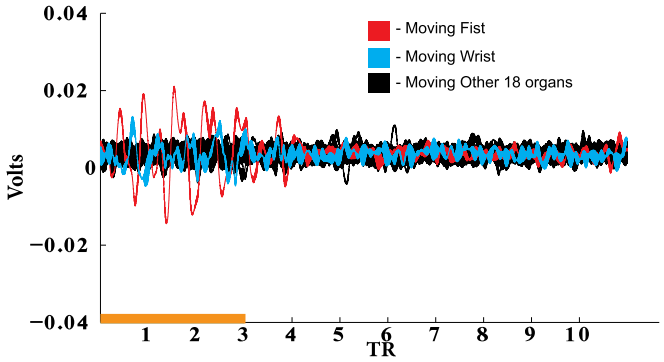

Fig. S2. EMG measurements from the biceps muscle of one subject when moving each of the 20 body parts in the slow event-related experiment. Orange, the duration of instructed movement.

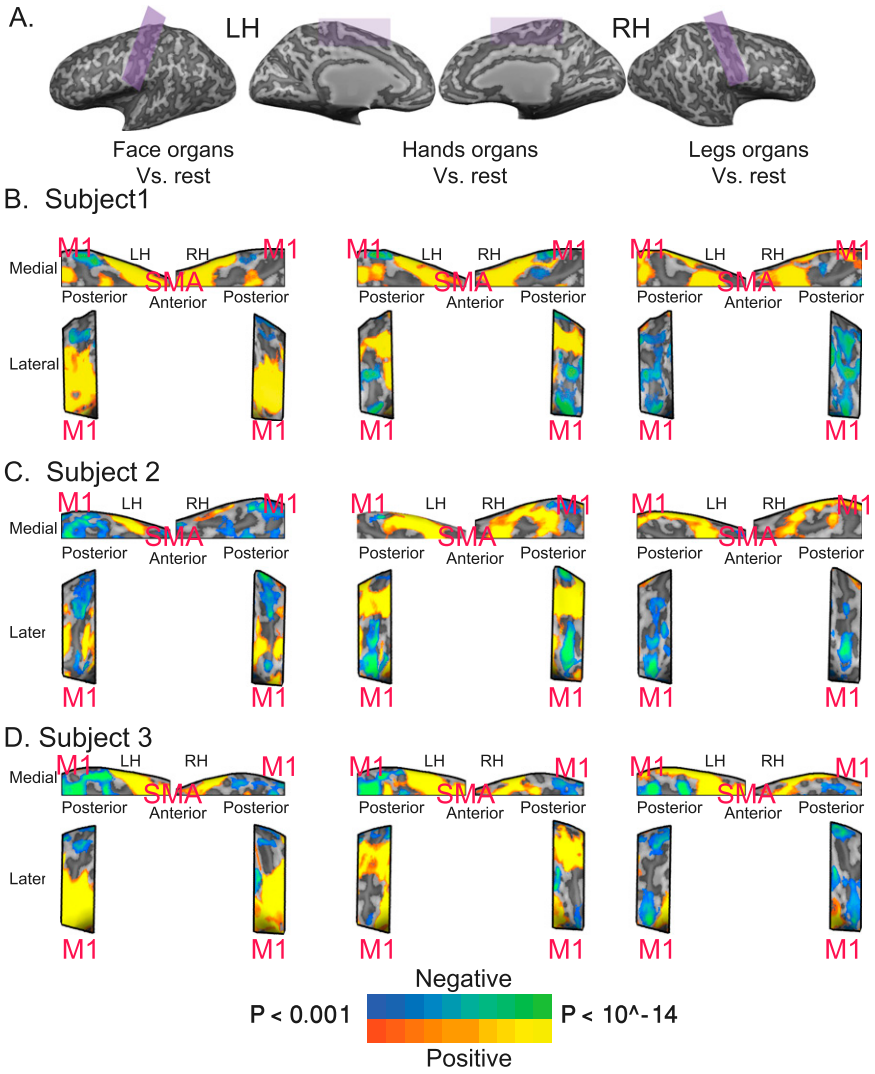

Fig. S3. (*A*) Anatomical display showing the areas enlarged in *B–D* (purple). (*B–D*) Statistical parametric maps for three subjects separately in the slow event-related experiment of face (*Left*), hand (*Center*), and leg body parts (*Right*).

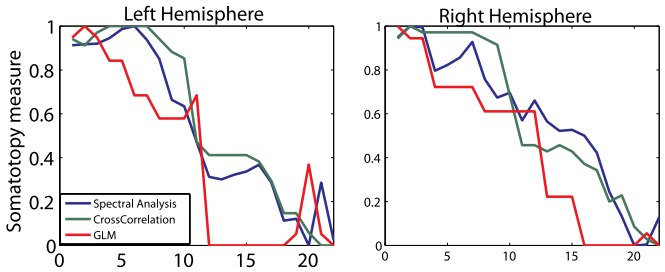

Fig. S4. The normalized somatotopy measure of cross-correlation analysis (lag value), spectral analysis (phase value), and GLM analysis (the body part with the highest *t* value) is shown in 22 ROIs along the primary motor cortex in the left and right hemispheres.

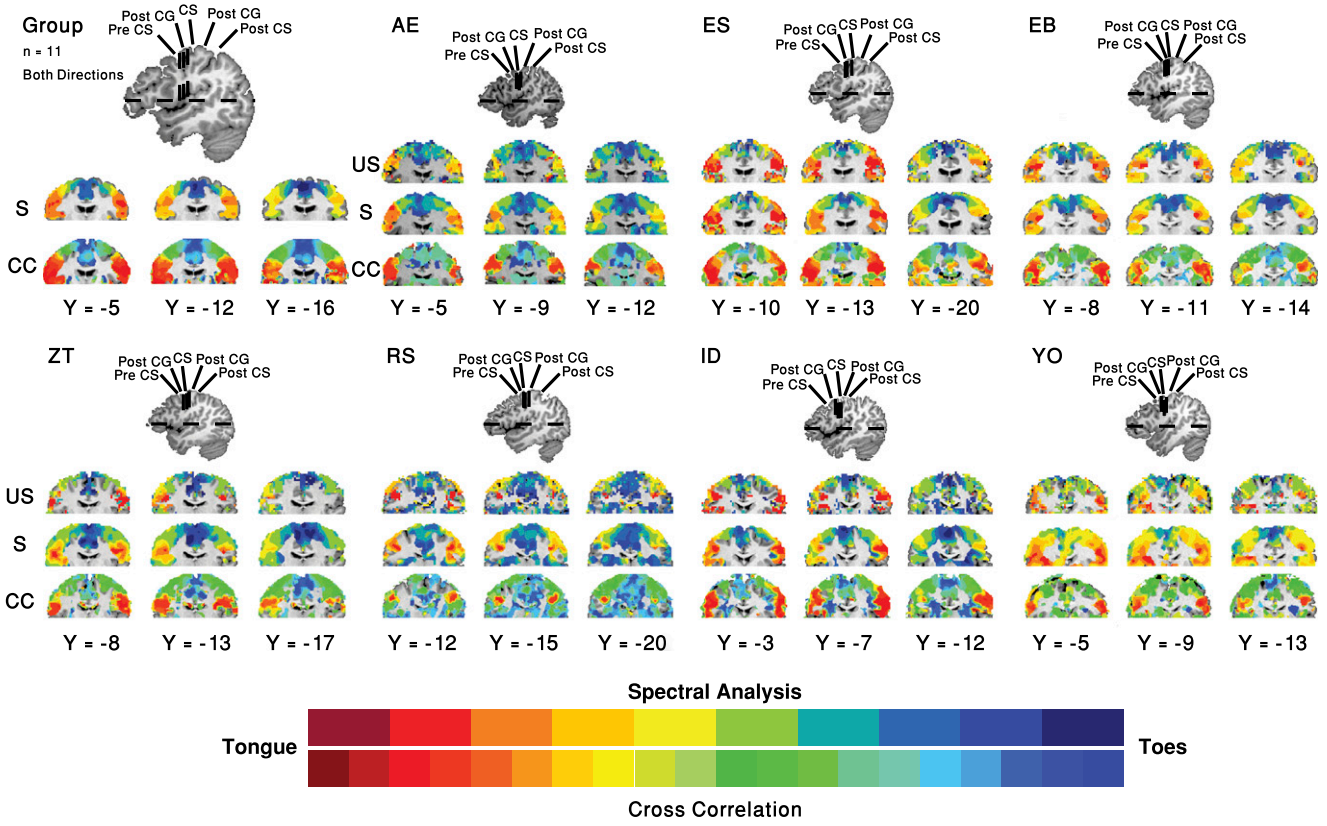

Fig. S5. Mapping M1 in single subjects using spectral analysis of the unsmoothed signal (US), smoothed signal (S), and cross-correlation analysis (CC).

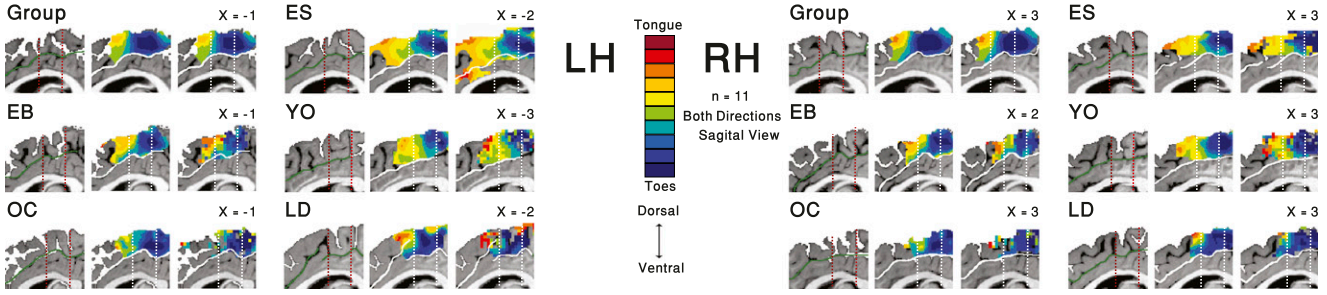

Fig. S6. Mapping the SMA in single subjects using spectral analysis of the unsmoothed signal (US), smoothed signal (S), and cross-correlation analysis (CC).

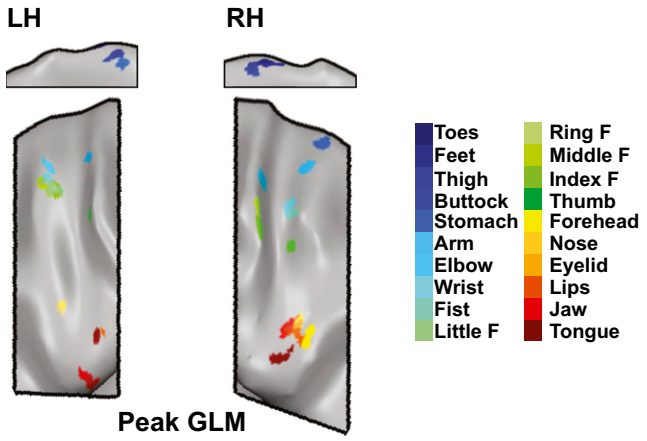

Fig. S7. Significant peak activations in M1 (19 peaks at the right hemisphere and 18 peaks at the left hemisphere) when contrasting each body part vs. all of the others masked by contrasting this body part with the rest (Table S1 shows the significance values).

Table S1. The *t* and *P* values of the contrasts in Fig. 1*A*, *Right*

	Peak thresholds			
	M1 right hemisphere		M1 left hemisphere	
	t	*P*	*t*	*P*
Toes	5.8	0.001	6.7	0.0005
Feet	7.2	0.0003	10.5	0.00004
Hips	8.5	0.0001	7.4	0.0003
Buttocks	7.4	0.0003	8.1	0.0001
Stomach	6.1	0.0008	5.1	0.002
Arm	5.5	0.001	8.1	0.0001
Elbow	8.3	0.0001	10.8	0.00003
Wrist	8.2	0.0001	10.7	0.00003
Fist	13	0.00001	13	0.00001
Little finger	6.8	0.0004	5.9	0.001
Ring finger	6.3	0.0007	7.3	0.0003
Middle finger	6.5	0.0006	6.3	0.0007
Index finger	4.7	0.003	2.55	0.04
Thumb	4.2	0.005	4.6	0.003
Forehead	4.5	0.004	2	0.09 (NS)
Nose	7.1	0.0003	4.6	0.003
Eyelids	1.9	0.1 (NS)	0.9	0.4 (NS)
Lips	6.9	0.0004	4.8	0.003
Jaw	6.3	0.0007	5.7	0.001
Tongue	8.6	0.0001	7.3	0.0003

The *t* and *P* values for the separate contrasts for each body part and hemisphere. Each body part was contrasted against all others and masked by this body part vs. the rest. NS, not significant.

Table S2. The *t* and *P* values of the contrasts in Fig. 1*E*

	Peak thresholds			
	SMA right hemisphere		SMA left hemisphere	
	t	*P*	*t*	*P*
Toes	6.3	0.0007	6.9	0.0004
Feet	8.5	0.0001	10.1	0.00005
Hips	9.1	0.00009	8.6	0.0001
Buttocks	10.5	0.00004	10.6	0.00004
Stomach	8.8	0.0001	9.2	0.00009
Arm	8	0.0002	10.1	0.00005
Elbow	8.8	0.0001	9.59	0.00007
Wrist	10.5	0.00004	11.9	0.00002
Fist	13.5	0.00001	15.7	0.000004
Little finger	8.2	0.0001	9.7	0.00006
Ring finger	8.9	0.0001	11	0.00003
Middle finger	13.3	0.00001	19.1	0.000001
Index finger	10.5	0.00004	10.6	0.00004
Thumb	9.1	0.00009	9.1	0.00009
Forehead	8.3	0.0001	9	0.0001
Nose	10.8	0.00003	11.5	0.00002
Eyelids	6.3	0.0007	7.6	0.0002
Lips	10.6	0.00004	11.4	0.00002
Jaw	7.2	0.0003	8.2	0.0001
Tongue	11.1	0.00003	9.8	0.00006

The *t* and *P* values for the separate contrasts for each body part and hemisphere. Each body part was contrasted against rest.